Electrochimica Acta 117 (2014) 292–298

Contents lists available at ScienceDirect

Electrochimica Acta

journal homepage: www.elsevier.com/locate/electacta

Ethanol Oxidation Reaction Using PtSn/C+Ce/C Electrocatalysts: Aspects of Ceria Contribution

R.F.B. De Souza [a], J.C.M. Silva [a], M.H.M.T. Assumpção [a], A.O. Neto [b], M.C. Santos [a,*]

[a] LEMN–Laboratório de Eletroquímica e Materiais Nanoestruturados–CCNH–Centro de Ciências Naturais e Humanas, UFABC–Universidade Federal do ABC, CEP 09.210-170, Rua Santa Adélia 166, Bairro Bangu, Santo André, SP, Brasil
[b] Instituto de Pesquisas Energéticas e Nucleares, IPEN, CNEN/SP, Av. Prof. Lineu Prestes, 2242 Cidade Universitária, CEP 05508-900, São Paulo, SP, Brazil

ARTICLE INFO

Article history:
Received 21 November 2013
Accepted 22 November 2013
Available online 4 December 2013

Keywords:
Ethanol oxidation reaction
electrocatalysis
platinum tin alloys
ceria
polymeric precursor method

ABSTRACT

The ethanol oxidation reaction (EOR) was investigated using PtSn/C + Ce/C electrocatalysts in different mass ratios (58:42, 53:47, and 42:58) prepared using the polymeric precursor method. Transmission electron microscopy (TEM) experiments showed particles sizes in the range of 3 to 7 nm. Changes in the net parameters observed for Pt suggest the incorporation of Sn into the Pt crystalline network with the formation of an alloy mixture with the SnO_2 phase. Among the PtSn/C + Ce/C catalysts investigated, the 53:47 composition showed the highest activity towards the EOR. In this case, the j versus t curves obtained in the presence of ethanol in acidic media exhibited a current density 90% higher than that observed with the commercial PtSn/C (ETEK). Correspondingly, during the experiments performed on single direct ethanol fuel cells, the maximum power density obtained using PtSn/C + Ce/C (53:47) as the anode was approximately 60% higher than that obtained using the commercial catalyst. FTIR data showed that the observed behavior for ethanol oxidation may be explained in terms of a synergic effect of bifunctional mechanism with electronic effects, in addition to a chemical effect of ceria that provides oxygen-containing species to oxidize acetaldehyde to acetic acid.

1. Introduction

The ethanol oxidation reaction (EOR) has been recognized as an important topic because of its role in direct ethanol fuel cells (DEFCs). The use of ethanol as a fuel provides certain advantages, specifically a high energy density, a liquid state at room temperature, low toxicity and the ability to be produced from biomass [1–3].

Carbon-supported platinum is commonly used as an anode catalyst in low-temperature fuel cells. However, pure platinum is not the most efficient anodic catalyst because it is rapidly poisoned by strongly adsorbed species generated from the dissociative adsorption of ethanol [4,5]. Binary Pt-based electrocatalysts with a second metal have been found to circumvent this problem. The requirements for the second metal are as follows: it must have a greater ability to form surface oxygen-containing species at potentials less positive than those required to form oxygen-containing species on Pt (the bi-functional effect) [6–9], and it must modify the d-band levels and thereby change the electron density of Pt (the electronic effect) [9–11].

Numerous studies have indicated that PtSn/C is the best binary catalyst for the EOR [12–16]. However, discrepant viewpoints have focused on whether the effects obtained with this electrocatalyst are obtained through the alloying of Pt with Sn or through the combination of Pt with SnO_2 [2,16–18]. According to Antolini *et al.* [19,20], the maximum activity of a PtSn material for the EOR depends on the ratio between alloyed and non-alloyed tin.

In contrast, CeO_2 has been extensively used in three-way catalysts, the water–gas-shift reaction, fuel cells, and solar cells [21–27]. CeO_2 is a fluorite-structured oxide with a high oxygen storage capacity (OSC) associated with its extensive oxygen vacancies, the low redox potential between Ce^{3+} and Ce^{4+}, and its electrical properties [21,28,29].

The synergic effect of ceria and tin has been studied by Neto *et al.* [30–33]. When ceria was studied as a support with carbon, PtSn/CeO_2-C electrocatalysts were shown to be more active for the EOR than the analogous PtSn/C catalysts, and the better performance was attributed to the oxygen-containing species generated by ceria that assist PtSn in the EOR [30,31,33].

Recently, the effect of ceria as an catalyst in a ternary material (PtSnCe/C) was investigated [32], and the results showed that the optimal composition of PtSnCe/C (68:22:10) exhibited the highest activity toward the EOR—activity higher than that observed for commercial PtSn/C (E-Tek), which was attributed to the oxygen-containing species that oxidize ethanol to acetic acid.

* Corresponding author. Tel.: +55 11 4996 0163; fax: +55 11 4996 0090.
E-mail addresses: mauro.santos@ufabc.edu.br, drmcsa@gmail.com (M.C. Santos).

0013-4686/$ – see front matter © 2013 Elsevier Ltd. All rights reserved.
http://dx.doi.org/10.1016/j.electacta.2013.11.129

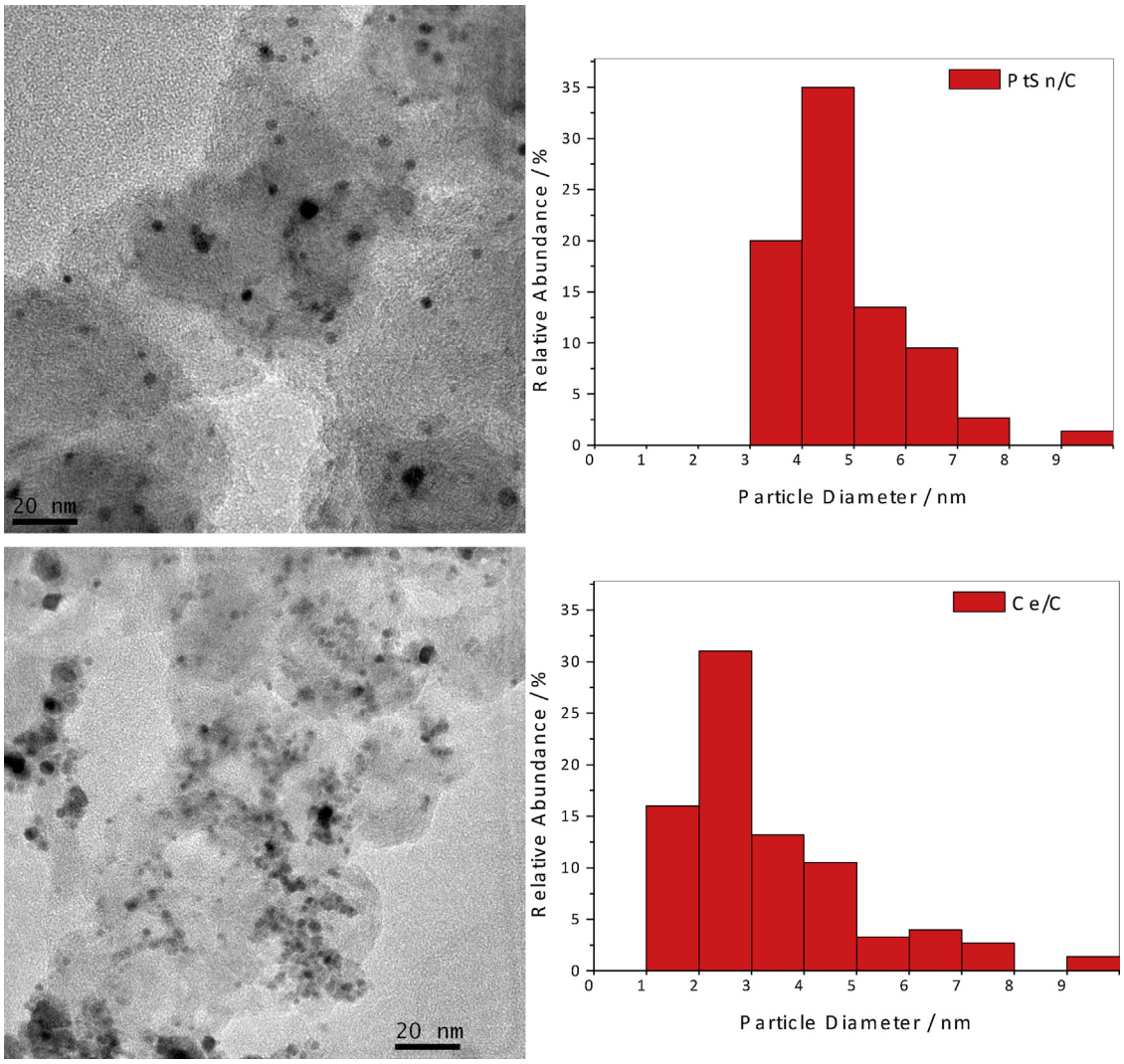

Fig. 1. Histogram of the catalyst particle mean diameter distribution and TEM micrographs of the Pt_3Sn/C and Ce/C electrocatalysts, as indicated in the figure.

Silva *et al.* [12] noted during their investigation of PtSn alloyed and non-alloyed materials for the EOR, that the electrocatalyst with largest lattice parameters for Pt produced more acetic acid with faster kinetics than did materials with smaller lattice parameters for Pt; these results agree with those of Colmati *et al.* [20]. Consequently, these lattice parameters can influence in the electrocatalytic activity for the EOR and thereby prevent the elucidation of the role of CeO_2 in the electrocatalyst.

The oxygen atoms present in the lattice of CeO_2 are expected to be either directly or indirectly involved in promoting the removal of the intermediary that is formed on Pt [29] and/or on PtSn during the ethanol electrooxidation.

In this work, composites of PtSn(3:1)/C + Ce/C catalysts were designed for an EOR anode. Using this material, we expected that the concomitant use of PtSn and ceria could produce a synergetic effect and result in high-activity electrocatalysts. Furthermore, we intended to discover the role of ceria in the EOR by maintaining the PtSn fraction in terms of both constant composition and lattice parameter; the only variable with respect to the electrocatalysts analyzed was the amount of CeO_2. The materials were prepared using the polymeric precursor method, and the electrocatalytic activity toward the EOR was examined through experiments using chronoamperometry and single direct ethanol fuel cells. The pathways for ethanol oxidation on the $Pt_3Sn/C + CeO_2/C$ electrocatalysts were also investigated by *in situ* ATR-FTIR spectroscopy to obtain information about intermediates, reaction products and the capability to produce a material with good catalytic activity compared to that of PtSn/C.

2. Experimental

The Pt:Sn 3:1 (40% w/w) and Ce (5% w/w), both of which were prepared on carbon XC-72, were prepared using a modified polymeric precursor method (PPM). For further details, see [2,12,26,32] and references therein. For this purpose, a mass ratio of 1:50:400 (metallic precursor: citric acid (CA): ethylene glycol (EG)) was used to prepare the polymeric resin. Chloroplatinic acid ($H_2PtCl_6.6H_2O$, Sigma-Aldrich), tin(II) chloride ($SnCl_2.2H_2O$, Merck) and cerium(III) chloride ($CeCl_3$, Merck) were used as precursors. After the precursors were calcined, the resulting powders were mixed in three compositions, 58:42, 53:47, and 42:58, to obtain metal compositions of 69:23:8, 68:22:10, and 64:21:15 (Pt:Sn:Ce) with $23 \pm 2\%$ (w/w) metal/carbon loading.

All of the electrocatalysts were characterized by X-ray diffraction (XRD) performed on a Rigaku model Miniflex II diffractometer equipped with a Cu Kα radiation source ($\lambda = 0.15406$ nm). The diffractograms were recorded from $2\theta = 20^\circ$ to 90° with a step size of 0.05° and a scan time of 2 s per step. Transmission electron

microscopy (TEM) was performed on a JEOL JEM-2100 electron microscope operated at 200 kV, which was used to determine the morphology, distribution, and size of the nanoparticles in the support. The mean particle sizes were determined from more than 200 particles from different regions of each sample.

Electrochemical measurements were performed at room temperature (T = 25 °C) using an Autolab PGSTAT 302 N potentiostat. Glassy carbon (GC) with a geometric area of 0.071 cm^2 was used as a support for the working electrodes. A Pt sheet and a reversible hydrogen electrode were used as the counter electrode and reference electrode, respectively. For the construction of the working electrodes, 8 mg of electrocatalyst powder was dispersed in 1 ml water and mixed for 5 min in an ultrasonic bath. Afterwards, 20 μl of Nafion® solution (5%) was added, and the suspension was again mixed in an ultrasonic bath for 15 min. Aliquots of 5 μl of the dispersion were pipetted onto the glassy carbon support surface. The electrode was subsequently dried at 60 °C for 20 min and was finally hydrated for 5 min in water. The chronoamperometric experiments were performed in 0.1 mol L^{-1} $HClO_4$ solution in the presence of 1 mol L^{-1} of ethanol. The electrochemical cell was purged for 15 min with N_2 before each experiment.

Direct ethanol fuel cell tests were performed using $Pt_3Sn/C + CeO_2/C$ electrocatalysts as anodes and Pt/C electrocatalysts as cathodes. For DEFC studies, Teflon-treated carbon cloth (Electrochem ECCC1-060 T) was used as a gas diffusion layer, and a Nafion ® 117 membrane was used as the electrolyte. The electrodes (anode or cathode) were hot pressed onto both sides of a Nafion ®117 membrane at 100 °C for 2 min under a pressure of 225 kgf cm^{-2}. The prepared electrodes contained 1 mg Pt cm^{-2} in the anode and cathode. The 2 M ethanol aqueous solution was delivered at approximately 2 mL min^{-1}, and the oxygen flow was set to 500 mL min^{-1} under 2 bar of pressure.

The spectroelectrochemical ATR-FTIR *in situ* measurements were performed using the same working electrodes used in the chronoamperometry experiments. The measurements were performed on a Varian® 660 IR spectrometer equipped with a MCT detector cooled with liquid N_2, an ATR accessory (MIRacle with a Diamond/ZnSe Crystal Plate Pike®) and a special cell [12] at 25 °C in presence of 0.1 mol L^{-1} $HClO_4$ in 1.0 mol L^{-1} ethanol. The absorbance spectra were collected as the ratio R:R_0, where R represents a spectrum at a given potential, and R_0 is the spectrum collected at 0.05 V. The positive and negative directional bands represent the gain and loss of species at the sampling potential, respectively. The spectra were computed from 128 interferograms averaged from 2500 cm^{-1} to 850 cm^{-1} with the spectral resolution set to 8 cm^{-1}. Initially, a reference spectrum (R_0) was measured at 0.05 V, and the sample spectra were collected after successive potential steps from 0.2 V to 1.0 V were applied [3,12,34].

3. Results and Discussion

3.1. Characterization of Pt_3Sn/C and Ce/C

Figure 1 presents TEM micrographs and histograms for the particles of the PtSn/C and Ce/C electrocatalysts. Well-dispersed particles in the support were observed in all of the electrocatalysts, although some agglomerates were also observed. For the Pt_3Sn/C material, the average particle size was 4.0 ± 1.5 nm, whereas for Ce/C, the average particle size was 3.0 ± 1.0 nm. In addition, the particle sizes found for our catalysts are in agreement with those previously reported for platinum–tin [2,18,35–37].

Figure 2a shows the XRD patterns for the PtSn/C catalysts (the Pt peak positions were inserted for the reference standard). The XRD patterns for PtSn/C indicate the presence of the face-centered cubic (fcc) structure of platinum, with a slight shift in the

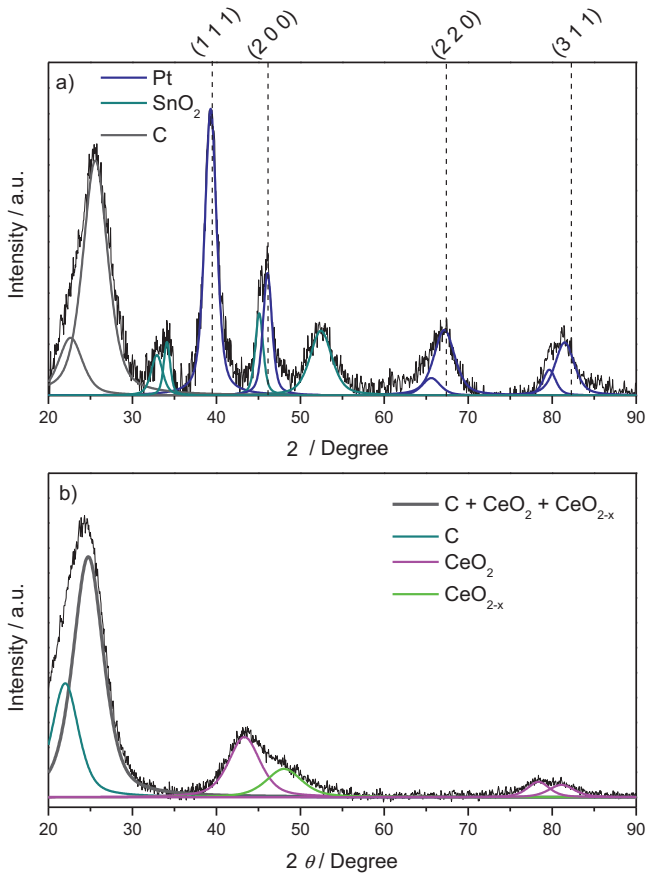

Fig. 2. X-ray diffraction patterns of the a) Pt_3Sn/C and b) Ce/C materials.

positions of the peaks (to lower 2θ values) caused by a change in the lattice parameters due to the incorporation of Sn atoms. The peak that corresponds to the plane 220 is asymmetric, and the deconvolution process [9] revealed two components: one of them (2θ = 67.22° and 0.3933 nm) exhibits parameters close to those of bulk Pt (2θ = 67.51° and 0.3911 nm), whereas the second suggests a higher degree of alloying (2θ = 65.79° and 0.4001 nm). Additionally, diffraction signals were observed at 2θ values at approximately 33° and 51° for this material that were attributed to SnO_2 (JCPDF # 41-1445). Figure 2b shows the XRD patterns for the CeO_2/C, and this material contained two different phases: CeO_2 and CeO_{2-x}. The characteristic diffraction peaks were attributed to CeO_2 (2θ = 28.6°) and CeO_{2-x} (2θ = 43.2°) based on JCPDF #65-5923 and JCPDF #49-1415, respectively. These two phases of cerium oxide were also observed by Assumpção *et al.* [38,39] when they prepared Ce/C with a low metal/carbon loading.

The mean crystallite sizes of PtSn/C and Ce/C based on the peak associated to the (220) plane were 4 nm for PtSn/C and 2 nm for Ce/C; these results are similar to the sizes obtained from the TEM images. The Ce/C particle size was smaller than that obtained by Yang *et al.* [23] (4 nm), who preparing CeO_x nanoparticles, and smaller than that reported by Serrano-Ruiz *el al.* [40] (3 nm), who studied ceria supported on active carbon.

To evaluate the electrocatalytic activity of PtSn/C + Ce/C materials, current–time curves were obtained during ethanol electrooxidation in an acidic medium; the results are shown in Fig. 3. The result for PtSn/C E-TEK was also included for purposes of comparison. All of the curves were normalized by the mass of Pt. For PtSn/C + Ce/C (53:47), the decay of the current is slower than that for the other catalysts. The current density measured for the EOR using this material after 30 minutes is approximately

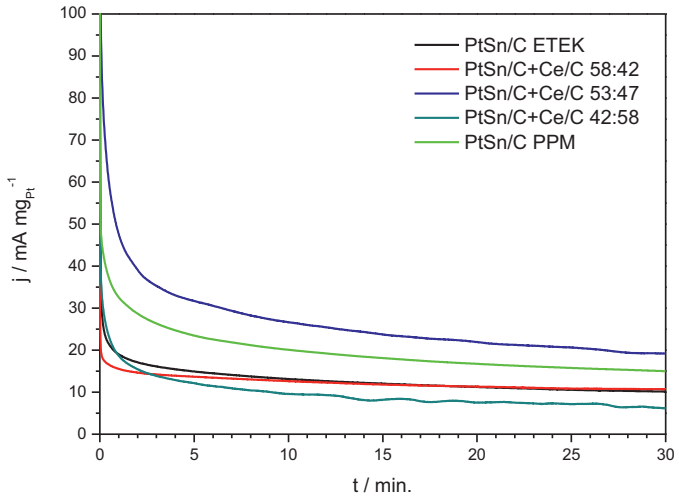

Fig. 3. Chronoamperogram for ethanol oxidation using PtSn/C + Ce/C in different ratios as electrocatalysts in 0.1 mol L^{-1} $HClO_4$ with 1 mol L^{-1} ethanol; E = 0.5 V vs. RHE.

19 mA mg_{Pt}^{-1}, which is approximately 2 times higher than the value obtained for the commercial material (9 mA mg_{Pt}^{-1}). The second material that is more active than the commercial material is PtSn/C prepared via the polymeric precursor method; this material exhibited a current density for the EOR approximately 60% higher than that exhibited by the commercial material.

The PtSn material, which was the base for all of the electrocatalysts, exhibits characteristics of an alloy and of a segregated oxide, as indicated by a change in the platinum electronic density associated with the formation Pt and Sn alloys [6,41,42]. This change in electronic density enables PtSn to modify the ethanol electrooxidation pathways by diminishing the adsorption strength of poisoning intermediates (e.g., CO) on the Pt sites. Furthermore, by keeping the surface free to promote new cycles of adsorption and electrooxidation, PtSn promotes a bifunctional mechanism, where Pt acts on ethanol adsorption and dissociation, while tin oxide and ceria provide oxygenated species at lower potentials for oxidative removal of the adsorbed intermediates formed during ethanol oxidation [26,29,30]. This assumption is in agreement with the results of Shibio *et al.* [28] and other authors [43–45], who claim that the bifunctional mechanism could be favored by a synergistic effect between ceria and tin sites because cerium oxide is well known in heterogeneous catalysis as a good source of oxygenated species that may favor ethanol oxidation [26]. This assumption is also in agreement a synergic combination of both of the previously discussed effects, as a reported by De Souza *et al.* [32] in their study of PtSnCe/C for the EOR.

These effects are attributed to an optimal composition between the PtSn/C and Ce/C. The optimal composition is commonly attributed, as required, to the bifunctional mechanism [46,47], and the literature on this effect includes work on electrocatalysts that contain ceria for the electrooxidation of methanol or ethanol [26,30,32]. These previously published results can explain the results observed with other compositions. In this case, the optimal composition cannot be attributed to the covering of sites because of the nature of the material prepared; it can, however, possibly be attributed to some other chemical or electrochemical effect that is not completely present when the material is prepared for only one step.

The performance of an electrocatalyst in a real fuel cell is of ultimate importance for its practical application, and the experiment with a single DEFC at 100 °C and with O_2 as the cathodic oxidant can effectively reflect the catalytic effect of the anode catalysts. Figure 4 shows the polarization and power density curves using, as anodes, PtSn/C + Ce/C (53:47), the most active material in the potentiostatic experiments; PtSn/C, which was the second-most active material and is also the material that gave the composites PtSn/C + Ce/C; and the commercial material PtSn/C ETEK as a reference curve.

The results in Fig. 4 show that the open-circuit potentials (OCV) of the two materials prepared for these studies are very similar (0.7 V and 0.71 V). When PtSn/C was used as the anode, the obtained maximum power density (35 mW cm^{-2}) was close to that obtained with the commercial material (33 mW cm^{-2}), respectively. However, the material that included ceria, when used as the anode, exhibited a maximum power density of 56 mW cm^{-2}, which represents a 60% increase over that of the original material. These results indicate that the inclusion of ceria–carbon on the electrocatalyst makes it more active. The literature also contains reports of the presence of ceria increasing the electrocatalytic activity for the EOR [29,31,32].

To correlate the activity of ethanol oxidation with the preferential pathway, we also used the ATR-FTIR *in situ* spectroscopy

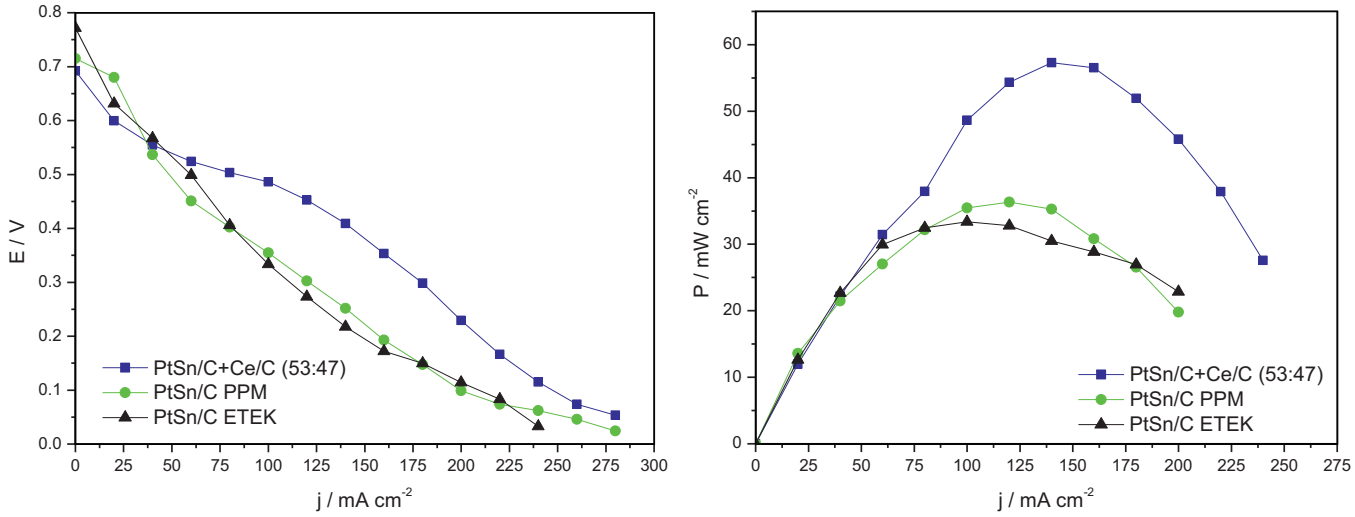

Fig. 4. Polarization curves (a) and power density curves (b) in a 5 cm^2 DEFC at 100 °C using PtSn/C + Ce/C and PtSn/C ETEK electrocatalysts as anode catalysts (1 mg Pt cm^{-2}) and Pt/C ETEK as the cathode catalyst (1 mg Pt cm^{-2}). Nafion® 117 was used as the membrane. Ethanol 2 mol L^{-1} with 2 mL s^{-1} flux.

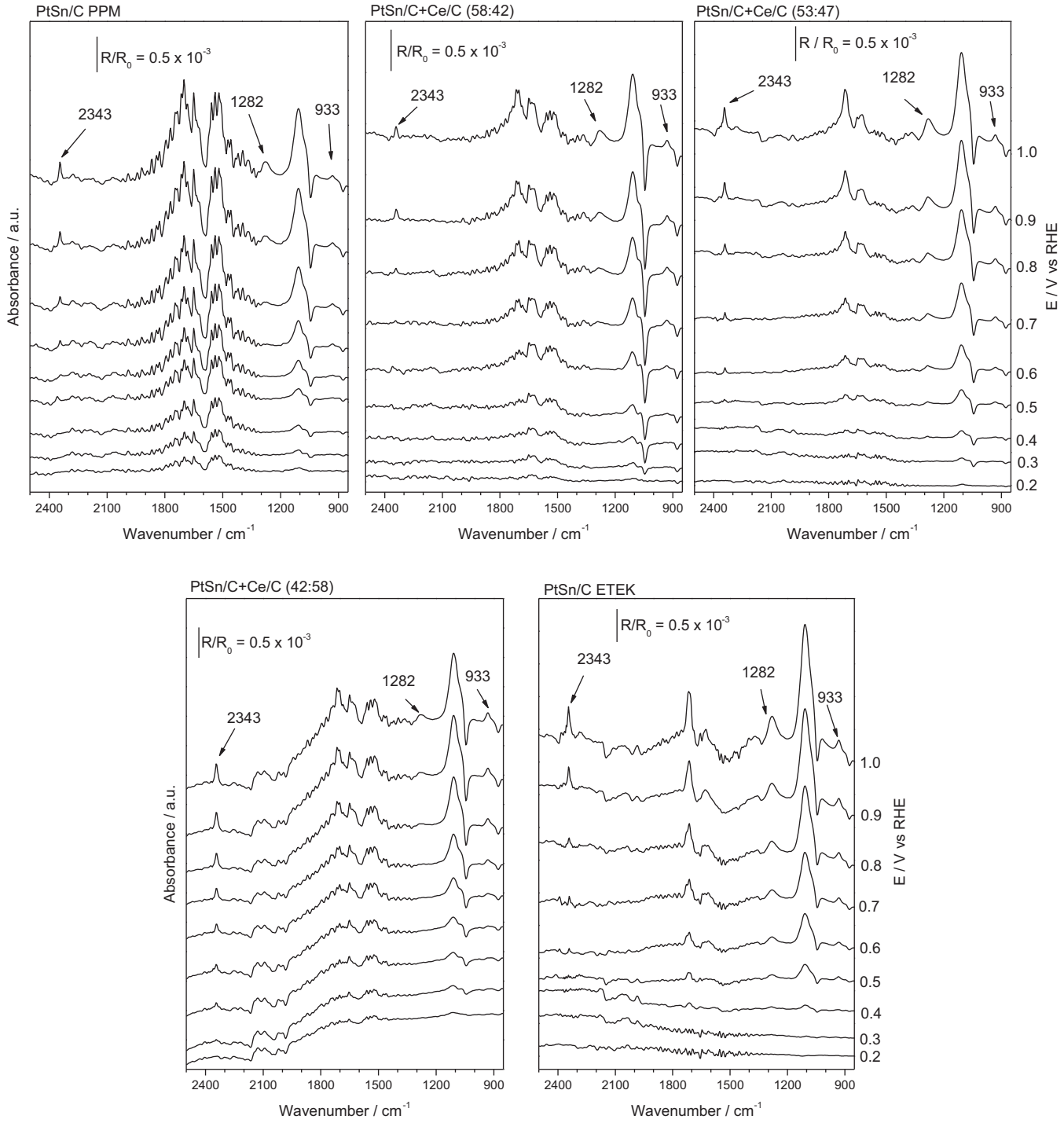

Fig. 5. *In situ* ATR-FTIR spectra taken between 0.2 and 1.0 V (RHE) using electrocatalysts that contained PtSn in 0.1 mol L^{-1} $HClO_4$ + 1.0 mol L^{-1} ethanol. The backgrounds were collected at 0.05 V *vs.* RHE.

technique. The results these experiments are presented in Figure 5. With this technique, the appearance of bands related to acetic acid (1280 cm^{-1}), acetaldehyde (933 cm^{-1}), CO_2 (2343 cm^{-1}), adsorptions of perchlorate anions (1130 cm^{-1}), carbonyl groups (1710 cm^{-1}), HOH deformation from water [48–51] and the consumption band of ν_a(CCO) that corresponds to ethanol [52] can be observed.

The FTIR spectra obtained for all of the electrodes suggested that different compositions of PtSn/C and Ce/C do not induce the occurrence of additional pathways of oxidation; the catalyst compositions therefore all result in the production of CO_2, acetic acid, and acetaldehyde. However, the potentials at which the bands of these species appear differ for each electrode.

To evaluate the effect of electrocatalysts on the product distribution during the EOR at different potentials, all of the bands were deconvoluted to Lorentzian line forms [3,12,34] and normalized using the band intensities at all potentials divided by the band intensity obtained at 1 V for each electrode [53]. Thus, the intensity and line width of each band could be individually analyzed. Figure 6

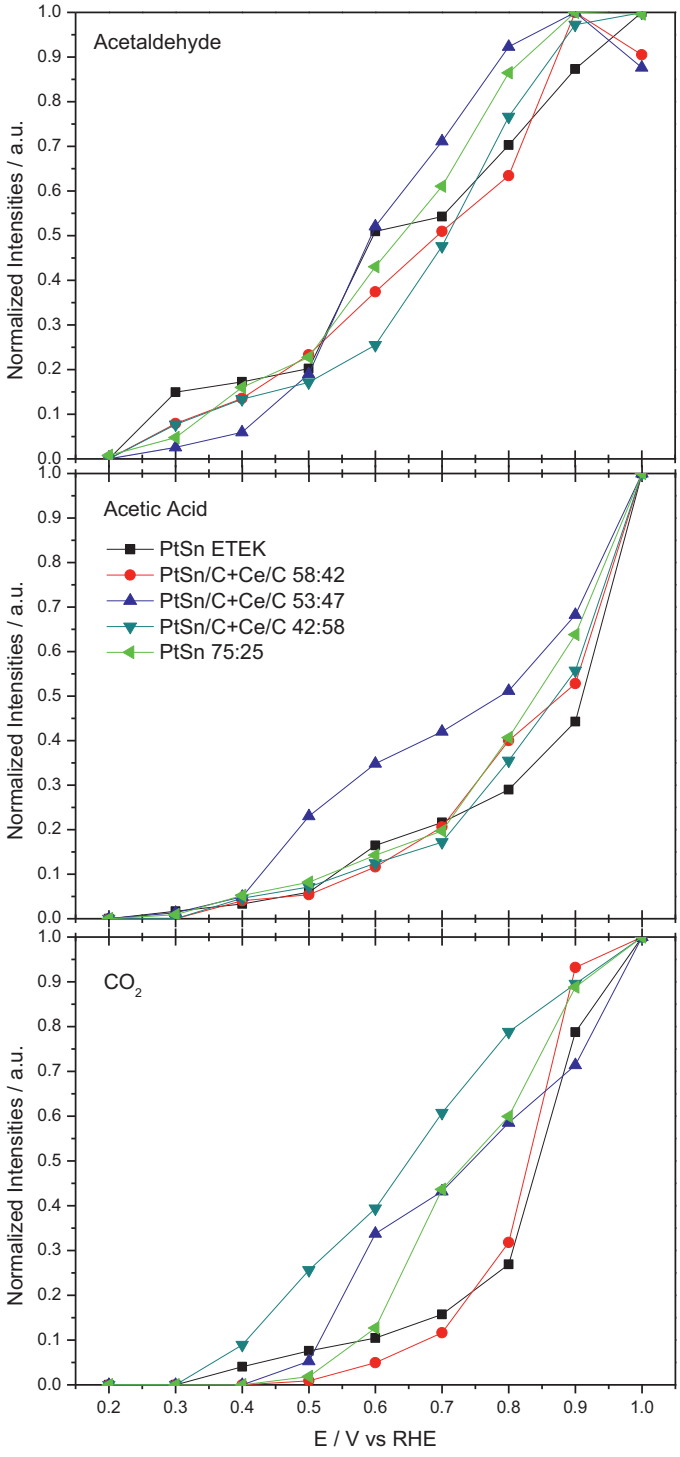

Fig. 6. Normalized intensities of the acetaldehyde, acetic acid and CO_2 bands as a function of the potential for the electrocatalysts. Data extracted from Fig. 5.

presents the normalized intensities of the acetic acid, acetaldehyde and CO_2 bands.

For all of the electrodes, acetaldehyde is the first product to appear, at 0.3 V, which is approximately 100 mV before to the emergence of the acetic acid and CO_2 signals. The appearance of the acetaldehyde band at an onset potential that was lower than that of the other products has also been reported in other studies in which different electrodes were used [32,53]. These similarities may indicate that the oxidation of ethanol to aldehyde requires less energy consumption than that required for the formation of acetic acid or CO_2. However, the formation of acetaldehyde at a low potential does not indicate that other products are formed only from it; Giz and Camara [53] have reported that ethanol can be oxidized to acetic acid on Pt (111) via parallel pathways.

When the formation of acetic acid is observed, the behavior of the material PtSn/C + Ce/C 53:47 for the production of acetic acid is distinct from that of the other materials. The production of acetic acid is kinetically favored over CO_2 production, which reflects the current measured during the potentiostatic experiments [12]. In this case, the incorporation of ceria into the catalysts increased the local oxygen concentration and thereby acted as an oxygen buffer, which resulting in the best electrocatalytic activity toward ethanol oxidation at its optimal composition [38,54].

We can also observe from Figure 6 that, as the Ce loading is increased, the amount of CO_2 formed increases, and the onset potential of this product shifts to less-positive potentials; these results suggest that the Ce or CeO_2 facilitates the breaking of the C-C bond. The presence of Ce apparently favors the conversion of alcohol to CO_2 compared to other electrocatalysts, which contradicts the low current density obtained in the electrochemical experiments. This contradiction can be explained by two hypotheses: i) the kinetics of C-C cleavage are slow, which results in low current densities [12] and ii) some researchers [23,55,56] have claimed that the oxidation of CO over ceria proceeds according to a radical mechanism through the interaction of CO molecules with adsorbed O_2^- radicals, and these radicals may process the oxidation of alcohol without the transfer of electrons to the electrochemical system. Notably, these features differ substantially from those found using the PtSnCe/C electrocatalysts prepared in one step [28]. In the PtSnCe/C electrocatalysts, the lattice parameter of Pt is not constant, and the CeO_{2-x} phase is not present in equilibrium with the CeO_2 phase to provide oxygen for the oxidation of strongly bound intermediates, such as CO_{ads}, during ethanol oxidation.

4. Conclusions

In this study, the effect of ceria on the electrocatalytic activity of PtSn for the EOR was investigated, and the results indicated that the addition of Ce/C to the PtSn/C electrocatalyst increases the EOR activity, probably because of oxygen provided by CeO_2/CeO_{2-x}. The main product obtained for the EOR when PtSn/C:Ce/C (42:58) was used was acetic acid. However, the PtSn/C:Ce/C mixture has an optimal ratio (42:58), as does the mixture PtSnCe/C (68:22:10). The increased amount of Ce/C in the electrocatalyst was observed to shift the onset potential of CO_2 production to less-positive potentials than that obtained using pure PtSn/C.

Acknowledgements

The authors wish to thank the Brazilian Funding Institution FAPESP (Processes Numbers: 12/03516-5, 10/04539-3, 13/01577-0, 10/16511-6), CNPq (150639/2013-9) and UFABC for their financial support. In addition, we wish to thank the Instituto Nacional de Ciência e Tecnologia (INCT) de Energia e Meio Ambiente (Process Number 573.783/2008–0).

References

[1] C. Xu, Z. Tian, P. Shen, S.P. Jiang, Electrochim. Acta 53 (2008) 2610–2618.
[2] R.F.B. De Souza, L.S. Parreira, D.C. Rascio, J.C.M. Silva, E. Teixeira-Neto, M.L. Calegaro, E.V. Spinace, A.O. Neto, M.C. Santos, J. Power Sources 195 (2010) 1589–1593.
[3] J.C.M. Silva, B. Anea, R.F.B. De Souza, M.H.M.T. Assumpcao, M.L. Calegaro, A.O. Neto, M.C. Santos, Journal of the Brazilian Chemical Society 24 (2013) 1553–1560.
[4] Q. He, S. Mukerjee, B. Shyam, D. Ramaker, S. Parres-Esclapez, M.J. Illan-Gomez, A. Bueno-Lopez, J. Power Sources 193 (2009) 408–415.

[5] K. Wang, H. Wang, S. Pasupathi, V. Linkov, S. Ji, R. Wang, Electrochimica Acta 70 (2012) 394–401.
[6] F. Colmati, E. Antolini, E.R. Gonzalez, Appl. Catal. B 73 (2007) 106–115.
[7] J. Liu, J. Cao, Q. Huang, X. Li, Z. Zou, H. Yang, J. Power Sources 175 (2008) 159–165.
[8] M.B. de Oliveira, L.P.R. Profeti, P. Olivi, Electrochem. Comm. 7 (2005) 703–709.
[9] J.C.M. Silva, R.F.B. De Souza, M.A. Romano, M. D'Villa-Silva, M.L. Calegaro, P. Hammer, A.O. Neto, M.C. Santos, Journal of the Brazilian Chemical Society 23 (2012) 1146–1153.
[10] I.-S. Park, K.-S. Lee, Y.-H. Cho, H.-Y. Park, Y.-E. Sung, Catal. Today 132 (2008) 127–131.
[11] S.S. Gupta, S. Singh, J. Datta, Materials Chemistry and Physics 116 (2009) 223–228.
[12] J.C.M. Silva, L.S. Parreira, R.F.B. De Souza, M.L. Calegaro, E.V. Spinacé, A.O. Neto, M.C. Santos, Appl. Catal. B 110 (2011) 141–147.
[13] E. Antolini, J. Power Sources 170 (2007) 1–12.
[14] D.R.M. Godoi, J. Perez, H.M. Villullas, J. Power Sources 195 (2010) 3394–3401.
[15] M.Y. Zhu, G.Q. Sun, S.Y. Yan, H.Q. Li, Q. Xin, Energy & Fuels 23 (2009) 403–407.
[16] J.H. Kim, S.M. Choi, S.H. Nam, M.H. Seo, S.H. Choi, W.B. Kim, Appl. Catal. B 82 (2008) 89–102.
[17] Z. Liu, L. Hong, S.W. Tay, Materials Chemistry and Physics 105 (2007) 222–228.
[18] F.L.S. Purgato, P. Olivi, J.M. Léger, A.R. de Andrade, G. Tremiliosi-Filho, E.R. Gonzalez, C. Lamy, K.B. Kokoh, J. Electroanal. Chem. 628 (2009) 81–89.
[19] E. Antolini, F. Colmati, E.R. Gonzalez, J. Power Sources 193 (2009) 555–561.
[20] F. Colmati, E. Antolini, E.R. Gonzalez, J. Electrochem. Soc. 154 (2007) B39–B47.
[21] D.-H. Lim, W.-D. Lee, D.-H. Choi, H.-I. Lee, Appl. Catal. B 94 (2010) 85–96.
[22] M. Takahashi, T. Mori, A. Vinu, D.R. Oa, H. Kobayashi, J. Drennan, Advances in Applied Ceramics: Structural, Functional & Bioceramics 107 (2008) 57–63.
[23] S. Yang, M. Besson, C. Descorme, Appl. Catal. B 100 (2010) 282–288.
[24] A.E. Galetti, M.F. Gomez, L.A. Arrúa, M.C. Abello, Appl. Catal. A 348 (2008) 94–102.
[25] E.C. Wanat, K. Venkataraman, L.D. Schmidt, Appl. Catal. A 276 (2004) 155–162.
[26] R.F.B. De Souza, A.E.A. Flausino, D.C. Rascio, R.T.S. Oliveira, E.T. Neto, M.L. Calegaro, M.C. Santos, Appl. Catal. B 91 (2009) 516–523.
[27] M. Faisal, S.B. Khan, M.M. Rahman, A. Jamal, K. Akhtar, M.M. Abdullah, Journal of Materials Science & Technology 27 (2011) 594–600.
[28] M.A. Scibioh, S.-K. Kim, E.A. Cho, T.-H. Lim, S.-A. Hong, H.Y. Ha, Appl. Catal. B 84 (2008) 773–782.
[29] T. Mori, D.R. Ou, J. Zou, J. Drennan, Progress in Natural Science: Materials International 22 (2012) 561–571.
[30] A.O. Neto, L.A. Farias, R.R. Dias, M. Brandalise, M. Linardi, E.V. Spinacé, Electrochem. Comm. 10 (2008) 1315–1317.
[31] R.F.B. De Souza, M.M. Tusi, M. Brandalise, R.R. Dias, M. Linardi, E.V. Spinace, M.C. dos Santos, A.O. Neto, Int. J. Electrochem. Sci. 5 (2010) 895–902.
[32] R.F.B. De Souza, L.S. Parreira, J.C.M. Silva, F.C. Simões, M.L. Calegaro, M.J. Giz, G.A. Camara, A.O. Neto, M.C. Santos, Int. J. Hydrogen Energy 36 (2011) 11519–11527.
[33] A.O. Neto, M. Linardi, D.M. dos Anjos, G. Tremiliosi, E.V. Spinace, J. Appl. Electrochem. 39 (2009) 1153–1156.
[34] R.F.B. De Souza, J.C.M. Silva, F.C. Simoes, M.L. Calegaro, A.O. Neto, M.C. Santos, International Journal of Electrochemical Science 7 (2012) 5356–5366.
[35] F. Colmati, E. Antolini, E.R. Gonzalez, Electrochim. Acta 50 (2005) 5496–5503.
[36] L. Jiang, G. Sun, Z. Zhou, W. Zhou, Q. Xin, Catal. Today 93-95 (2004) 665–670.
[37] M. Zhu, G. Sun, H. Li, L. Cao, Q. Xin, Chinese Journal of Catalysis 29 (2008) 765–770.
[38] M.H.M.T. Assumpção, A. Moraes, R.F.B. De Souza, I. Gaubeur, R.T.S. Oliveira, V.S. Antonin, G.R.P. Malpass, R.S. Rocha, M.L. Calegaro, M.R.V. Lanza, M.C. Santos, Appl. Catal. A 411–412 (2012) 1–6.
[39] M.H.M.T. Assumpção, A. Moraes, R.F.B. De Souza, M.L. Calegaro, M.R.V. Lanza, E.R. Leite, M.A.L. Cordeiro, P. Hammer, M.C. Santos, Electrochimica Acta 111 (2013) 339–343.
[40] J.C. Serrano-Ruiz, E.V. Ramos-Fernández, J. Silvestre-Albero, A. Sepúlveda-Escribano, F. Rodríguez-Reinoso, Materials Research Bulletin 43 (2008) 1850–1857.
[41] M. Zhu, G. Sun, Q. Xin, Electrochim. Acta 54 (2009) 1511–1518.
[42] S.C. Zignani, V. Baglio, J.J. Linares, G. Monforte, E.R. Gonzalez, A.S. Aricò, Electrochimica Acta 70 (2012) 255–265.
[43] J.W. Guo, T.S. Zhao, J. Prabhuram, R. Chen, C.W. Wong, J. Power Sources 156 (2006) 345–354.
[44] F. Raimondi, G.G. Scherer, R. Kotz, A. Wokaun, Angew. Chem. Int. Ed. 44 (2005) 2190–2209.
[45] W.J. Zhou, W.Z. Li, S.Q. Song, Z.H. Zhou, L.H. Jiang, G.Q. Sun, Q. Xin, K. Poulianitis, S. Kontou, P. Tsiakaras, J. Power Sources 131 (2004) 217–223.
[46] G.A. Camara, R.B. de Lima, T. Iwasita, Electrochem. Comm. 6 (2004) 812–815.
[47] G.A. Camara, R.B. de Lima, T. Iwasita, J. Electroanal. Chem. 585 (2005) 128–131.
[48] J.M. Léger, S. Rousseau, C. Coutanceau, F. Hahn, C. Lamy, Electrochim. Acta 50 (2005) 5118–5125.
[49] G.A. Camara, T. Iwasita, J. Electroanal. Chem. 578 (2005) 315–321.
[50] M. Li, A. Kowal, K. Sasaki, N. Marinkovic, D. Su, E. Korach, P. Liu, R.R. Adzic, Electrochim. Acta 55 (2010) 4331–4338.
[51] S.C.S. Lai, S.E.F. Kleijn, F.T.Z. Öztürk, V.C. van Rees Vellinga, J. Koning, P. Rodriguez, M.T.M. Koper, Catal. Today 154 (2010) 92–104.
[52] J. Raskó, M. Dömök, K. Baán, A. Erdőhelyi, Appl. Catal. A 299 (2006) 202–211.
[53] M.J. Giz, G.A. Camara, J. Electroanal. Chem. 625 (2009) 117–122.
[54] M. Li, A. Kowal, K. Sasaki, N. Marinkovic, D. Su, E. Korach, P. Liu, R.R. Adzic, Electrochimica Acta 55 (2010) 4331–4338.
[55] C.L. Campos, C. Roldán, M. Aponte, Y. Ishikawa, C.R. Cabrera, J. Electroanal. Chem. 581 (2005) 206–215.
[56] C. Li, K. Domen, K. Maruya, T. Onishi, J. Am. Chem. Soc. 111 (1989) 7683–7687.